

Journal of Materials Chemistry C

Accepted Manuscript



This article can be cited before page numbers have been issued, to do this please use: L. Zhao, S. Wang, J. Lv, J. Ding and L. Wang, *J. Mater. Chem. C*, 2017, DOI: 10.1039/C7TC03374E.



This is an Accepted Manuscript, which has been through the Royal Society of Chemistry peer review process and has been accepted for publication.

Accepted Manuscripts are published online shortly after acceptance, before technical editing, formatting and proof reading. Using this free service, authors can make their results available to the community, in citable form, before we publish the edited article. We will replace this Accepted Manuscript with the edited and formatted Advance Article as soon as it is available.

You can find more information about Accepted Manuscripts in the [author guidelines](#).

Please note that technical editing may introduce minor changes to the text and/or graphics, which may alter content. The journal's standard [Terms & Conditions](#) and the ethical guidelines, outlined in our [author and reviewer resource centre](#), still apply. In no event shall the Royal Society of Chemistry be held responsible for any errors or omissions in this Accepted Manuscript or any consequences arising from the use of any information it contains.

Solution Processible Red Iridium Dendrimers Containing Oligocarbazole Dendrons for Efficient nondoped and doped Phosphorescent OLEDs

Lei Zhao, Shumeng Wang, Jianhong Lü, Junqiao Ding,* Lixiang Wang*

*State Key Laboratory of Polymer Physics and Chemistry, Changchun Institute of
Applied Chemistry, Chinese Academy of Sciences, Changchun, 130022, P. R. China*

Abstract:

Solution processible red Ir dendrimers named R-D1, R-D2 and R-D3, which contain quinoline-based homoleptic complex as the core and oligocarbazole as the dendron, have been facilely and successfully designed and synthesized via a post-dendronization procedure. With the increasing dendron generation from R-D1 to R-D3, the intermolecular interactions and luminescence quenching in solid states are found to be effectively prevented because of the encapsulation from the outer dendrons. As a result, the third-generation dendrimer R-D3 achieves the best nondoped device performance, revealing a promising EQE of 10.5% (9.2 cd/A, 7.0 lm/W) with CIE coordinates of (0.67, 0.33). Furthermore, the doped devices of R-D3 show a wide doping concentration window in the range of 5-30 wt.%, and a maximum EQE as high as 18.3% (25.7 cd/A, 33.0 lm/W) is realized at an about 10 wt.% doping content. The results can compete well with vacuum-deposited small molecular red phosphors, representing an important progress on solution processible phosphorescent dendrimers with red emissions.

1. Introduction

The development of printing OLED displays requires highly efficient light-emitting materials suitable for some cost-effective wet methods, such as blade coating^{1,2} and inkjet printing.^{3,4} According to their topology structures, these solution processible emitters can be divided into three classes: small molecules,^{5,6} dendrimers⁷⁻⁹ and polymers.¹⁰⁻¹³ Compared with the other two, dendrimers have much greater potential since they possess not only the well-defined molecular structures of small molecules to favor the reproducibility of material synthesis and device fabrication, but also the good solution processibility of polymers to ensure the formation of high quality films via solution processing.

Up to now, a series of phosphorescent dendrimers have been successfully explored for red-,^{14,15} green-^{16,17} and blue-emitting^{18,19} phosphorescent OLEDs (PhOLEDs), in which the transition-metal complex acts as the emissive core to harvest both the generated singlet and triplet excitons in order to realize a theoretical 100% internal quantum efficiency. For example, when using a heteroleptic iridium (Ir) complex bis(2,4-diphenylquinolyl)iridium(acetylacetonate) [(PPQ)₂Ir(acac)] as the central core, we designed and synthesized red Ir dendrimers by only decorating its C^N ligand with different carbazole dendrons.¹⁴ The third-generation dendrimer red-G3 achieved a maximum external quantum efficiency (EQE) of 6.3% for the corresponding nondoped PhOLEDs, which was further improved to 11.9% in the presence of host. Considering the still existed intermolecular interactions in red-G3 to some degree, subsequently, a fully oligocarbazole-encapsulated red Ir complex D-(PPQ)₂Ir(acac)

was newly reported.¹⁵ In this case, both the C^N and O^O ligands of (PPQ)₂Ir(acac) were tethered with oligocarbazole, thus leading to a record-high nondoped device EQE of 11.1% (8.7 cd/A, 6.0 lm/W) accompanied by Commission International De L'Eclairage (CIE) coordinates of (0.67, 0.33). However, the obtained performance seems to be inferior to that of vacuum-deposited red phosphors,²⁰⁻²⁴ and simultaneously their synthesis remains a big challenge since the pre-dendronized ligands often show poor solubility in the polar solvents (e.g. 2-ethoxyethanol) during complexation.¹⁹ These problems leave us much room to optimize the molecular design and synthesis of red phosphorescent dendrimers for high-efficiency solution-processed PhOLEDs.

In this paper, we demonstrate novel solution processible red Ir dendrimers, where oligocarbazole up to the third generation can be facilely incorporated into the periphery of tris(2-thienyl-4-phenyl)iridium [Ir(Th-PQ)₃] through a post-dendronization route (Scheme 1). Instead of the heteroleptic one, a homoleptic red Ir complex Ir(Th-PQ)₃ is selected as the core based on several concerns as followed: i) Without affecting the photophysical property of Ir core, the reactive bromo groups are easily to be introduced into the C^N ligand other than the O^O one. So the homoleptic structure is expected to be favorable for the post-dendronization that allows the ease preparation and independent tuning of each component. ii) Different from the partly-adopted non-conjugated linkage between core and dendron in the previously-reported heteroleptic red Ir dendrimers, the conjugated linkage here could endow these newly-developed homoleptic dendrimers not only with enough

rigidity to keep the highly emissive nature of the core, but also with effective encapsulation to prevent the unwanted luminescent quenching in solid states. As for the resultant red Ir dendrimers R-D1, R-D2 and R-D3, the nondoped device efficiency is gradually enhanced from 5.1% (4.2 cd/A, 3.3 lm/W) to 10.5% (9.2 cd/A, 7.0 lm/W) with the increasing generation number. Moreover, a wide doping concentration window in the range of 5-30 wt.% is realized for the doped devices of the third-generation dendrimer R-D3, revealing a state-of-art EQE of 18.3% (25.7 cd/A, 33.0 lm/W) and CIE coordinates of (0.65, 0.34). To the best of our knowledge, this is the first report on solution processible red Ir dendrimers with comparable efficiency to vacuum-deposited small molecular phosphors.

2. Results and Discussion

2.1 Synthesis and characterization

A post-dendronization procedure is adopted for the synthesis of red Ir dendrimers R-D1 ~ R-D3 as depicted in Scheme 1. Starting from 2-amino-4'-bromobenzophenone, an acid-catalyzed Friedländer reaction was performed to afford the quinoline-based C^N ligand Th-PQ-Br. Then Th-PQ-Br was complexed with IrCl₃·3H₂O to produce the Ir core R-Br bearing three reactive bromo groups. On the other hand, a selective C-N coupling was carried out between 1,4-dibromobenzene and different oligocarbazoles to give the bromo-containing carbazole dendrons D1-Br, D2-Br and D3-Br, which were converted into the corresponding boronic esters D1-B, D2-B and D3-B, respectively. Finally, via Suzuki cross-coupling between R-Br and D1-Br,

D2-Br or D3-Br, the desired red Ir dendrimers R-D1, R-D2 and R-D3 were easily and successfully prepared in an acceptable moderate yield of 54-78%. Their molecular structures were fully characterized and confirmed by ^1H and ^{13}C NMR spectra, MALDI-TOF mass spectroscopy and elemental analysis. Meanwhile, these dendrimers are readily soluble in common organic solvents, such as chloroform, tetrahydrofuran, toluene and chlorobenzene, ensuring their capability to form high quality films *via* spin-coating. This is confirmed by their atomic force microscopy (AFM) topographic images (Figure S1 in ESI), where the films of R-D1 ~ R-D3 display a pinhole-free and smooth surface with a root-mean square (RMS) roughness of 0.77-0.81 nm. In addition, the decomposition temperature corresponding to a 5% weight loss is considerably up from 470 °C of R-D1 to 530 °C of R-D3 (Table 1). And no glass transition is detected for R-D3, which is different from R-D1 with a distinct glass transition temperature of about 199 °C. These observations imply that R-D3 is more thermally stable than R-D1, favorable for the long-term stability of PhOLEDs.

2.2 Photophysical properties

The UV-Vis and photoluminescence (PL) spectra in solutions for the red Ir dendrimers R-D1 ~ R-D3 are shown in Figure 1a. As one can see, all these dendrimers display two major absorption bands. Consistent with the literature,⁵ the intense absorption below 420 nm can be attributed to the spin-allowed ligand-centered (LC) transitions. And the absorption peaked at around 240 nm, characteristic of oligocarbazole, is increased with the increasing number of carbazole subunits.

Meanwhile, the weak bands in 450-590 nm are also found to be discernible, which are assigned to the metal-to-ligand charge-transfer (MLCT) transitions. The solution PL spectra of R-D1 ~ R-D3 are nearly independent on the dendron generation since they all have the same spectral profiles with similar emission peaks at 606-609 nm and PL quantum yields (PLQYs) of 0.40-0.42. This suggests that the emission is mainly from the central Ir core, and the extension of oligocarbazole does not affect its optical property in dilute solutions.

On going from solutions to films, a red shift of about 15-33 nm is observed for all the dendrimers, indicative of aggregation to some degree. Despite such a bathochromic trend, the emission maximum is obviously blue-shifted from 639 nm of R-D1 to 624 nm of R-D3 (Figure 1b). In fact, when the outer dendron becomes larger and larger, the emissive inner cores can be isolated more and more effectively because of the encapsulation from dendrons. Therefore, the intermolecular interactions between the emissive cores are expected to be reduced to prevent the luminescence quenching in solid states. To further confirm this point, their film transient PL spectra were measured (Figure 2), and the average lifetime was estimated based on a biexponential fit of the corresponding emission decay curve. Attributable to the reduced intermolecular interactions, it is found that R-D3 decays slowly with a lifetime of 0.92 μ s longer than those of R-D1 and R-D2 (0.54-0.59 μ s).

2.3 Electrochemical properties

Cyclic voltammetry (CV) was used to explore the dendrimers's electrochemical

properties. During the anodic scanning in dichloromethane, multiple quasi-reversible oxidation waves is observed for the red Ir dendrimers R-D1 ~ R-D3 (Figure 3). The first oxidation is reasonably from the inner Ir core, while the others are from the outer carbazole dendrons. During the cathodic scanning in *N,N*-dimethyl formamide, they all display three quasi-reversible reduction waves that originate from the quinoline-based C^N ligand. According to the onset values of the first oxidation and reduction potentials, the highest occupied molecular orbital (HOMO) and lowest unoccupied molecular orbital (LUMO) energy levels of R-D1 ~ R-D3 are determined to be -5.12 — -5.13 eV and -2.79 — -2.83 eV, respectively. Obviously, their HOMO/LUMO levels are almost independent on the carbazole generation, in well agreement with the similar PL spectra in solutions.

2.4 Electroluminescence properties

To evaluate the electroluminescence (EL) properties of the red Ir dendrimers R-D1 ~ R-D3, their nondoped devices with a configuration of ITO/PEDOT:PSS (40 nm)/dendrimers (45 nm)/TmPyPB (60 nm)/LiF (0.5 nm)/Al were firstly fabricated (Figure 4a). Here TmPyPB represents 1,3,5-tri[(3-pyridyl)-phen-3-yl]benzene, and is utilized as the electron-transporting and hole-blocking material. As can be clearly seen in Figure 4b, all the dendrimers emit strong and pure red lights with CIE coordinates of (0.67, 0.33). The values keep nearly unchanged under the varying voltages in the range of 4-10 V, and match well with the National Television System Committee (NTSC) standard for red subpixels (0.67, 0.33). Different from the film PL

counterparts showing an obvious hypsochromic shift from R-D1 to R-D3, the observed similar EL spectra are probably ascribed to a different excitation environment in devices. Despite of this, the maximum brightness is gradually elevated from 10290 cd/m² of R-D1 to 14810 cd/m² of R-D3 (Figure 4c). Correspondingly, the EQE is improved from 5.1% (4.2 cd/A, 3.3 lm/W) of R-D1 to 10.5% (9.2 cd/A, 7.0 lm/W) of R-D3 (Figure 4d). As discussed above, with the growing dendron generation, the intermolecular interactions and luminescence quenching can be effectively inhibited, which is responsible for the efficiency improvement.

Taking into account there exists aggregation even in R-D3, its doped devices were then assembled by doping R-D3 into 4,4',4''-tris(*N*-3-methylphenyl-*N*-phenylamino)triphenylamine(m-MTDATA). The device structure, EL spectra, current density-voltage-luminance curves and current efficiency-luminance-EQE curves are given in Figure 5, and the related data are tabulated in Table 2. We note that the turn-on voltage at 1 cd/m² is considerably lowered from 3.2 V of nondoped device to 2.4 V of doped ones. Consistent with our previous report,²⁵ the formation of the interfacial exciplex between m-MTDATA and TmPyPB contributes to the decreased voltage, whose energy could be completely transferred to the dopant R-D3. This is verified by the EL spectra (Figure 5b), in which only the red emission from R-D3 is observed without any emissions from m-MTDATA, TmPyPB or m-MTDATA/TmPyPB exciplex. More interestingly, unlike small molecular phosphors, R-D3 realizes a very wide doping concentration window for doped devices. For example, when the doping concentration is up from 5 wt.% to

30 wt.%, the peak current efficiency varies in a shallow range of 22.7-25.7 cd/A. An only 11.7% variation is very beneficial for the reliability and reproducibility of commercial devices. On one hand, according to the literature,^{14, 18} the dendritic phosphor could perform well at high doping concentration because of the reduced intermolecular interactions after dendron encapsulation. On the other hand, the formed m-MTDATA/TmPyPB interfacial exciplex is a similar low exchange energy system to the thermally activated delayed fluorescence (TADF) host.²⁶ In this case, the promoted upconversion from triplet to singlet excitons may facilitate the long-range Förster energy transfer from host to dopant and spare the short-range Dexter to lower the dopant content. Therefore, the achievement of high efficiency even at low doping concentration is also reasonable and understandable. In addition, the best doped device performance is obtained at an about 10 wt.% doping concentration, revealing a maximum brightness of 25270 cd/m², a maximum current efficiency of 25.7 cd/A, a maximum power efficiency of 33.0 lm/W, a maximum EQE of 18.3% and CIE coordinates of (0.65, 0.34). Even at a luminance of 1000 cd/m², the EQE still remains to be as high as 17.0% (23.9 cd/A, 23.4 lm/W), indicative of gentle efficiency roll-off. To our knowledge, the reported performance here is among the highest for solution processible red dendrimers, and competes well with vacuum-deposited small molecular phosphors.

3. Conclusions

In summary, we report the synthesis, characterization and application of solution

processable red Ir dendrimers R-D1 ~ R-D3 by using a quinoline-based homoleptic complex as the emissive core and oligocarbazole as the dendron. Owing to the effective encapsulation from the outer dendrons and high emissive nature of the core, the third-generation dendrimer R-D3 shows a state-of-art EQE of 10.5% (9.2 cd/A, 7.0 lm/W) and 18.3% (25.7 cd/A, 33.0 lm/W) for its corresponding nondoped and doped devices, respectively. Given the comparable efficiency to vacuum-deposited small-molecular red phosphors, we believe that this work will promote the development of efficient red phosphorescent dendrimers for solution-processed PhOLEDs.

4. Experimental section

General information:

^1H and ^{13}C NMR spectra were recorded with a Bruker Avance 400 NMR spectrometer. MALDI/TOF mass spectra were obtained on an AXIMA CFR MS apparatus (COMPACT). Elemental analyses of carbon, hydrogen, and nitrogen were performed on a Bio-Rad elemental analysis system. AFM characterization was performed on SPA300HV with a SPI3800N controller (Seiko Instruments Inc., Japan) in a tapping mode. Thermal gravimetric analysis (TGA) and differential scanning calorimetry (DSC) were performed on Perkin Elmer-TGA 7 and Perkin Elmer-DSC 7 system under nitrogen at a heating rate of $10\text{ }^\circ\text{C min}^{-1}$. The UV-Vis absorption and PL spectra were measured by a Perkin-Elmer Lambda 35 UV/vis spectrometer and a Perkin-Elmer LS 50B spectrofluorometer, respectively. The PLQYs were measured in

N₂-saturated toluene solutions by a relative method using *fac*-Ir(ppy)₃ ($\Phi_p = 0.97$ in toluene) as the reference. The transient PL spectra were measured in N₂ atmosphere by exciting the samples with 355 nm light pulses with ca. 3 ns pulse width from a Quanta-Ray DCR-2 pulsed ND:YAG laser. And the average lifetimes were calculated according to the equation: $\tau_{av} = (A_1\tau_1^2 + A_2\tau_2^2) / (A_1\tau_1 + A_2\tau_2)$. Cyclic voltammetry (CV) measurements were obtained in anhydrous dichloromethane and degassed N,N-dimethyl formamide with *n*-Bu₄NClO₄ (0.1 mol L⁻¹) as the electrolyte on a CHI660a electrochemical analyzer under a scan rate of 100 mV s⁻¹. A glass carbon electrode, a Ag/AgCl electrode and a Pt wire were used as the working electrode, the reference electrode and the counter electrode, respectively.

Device fabrication and measurement:

Patterned glass substrates coated with indium tin oxide (ITO) were cleaned with acetone, detergent and distilled water, and then in an ultrasonic solvent bath. After baking in a heating chamber at 120 °C for 8 h, the ITO-glass substrates were treated with O₂ plasma for 30 min. Subsequently, poly(3,4-ethylenedioxythiophene):poly(styrenesulfonate) (PEDOT:PSS, Batron-P4083, Bayer AG) was spin-coated on top of the ITO at a speed of 5000 rpm for 60 s and then baked at 120 °C for 45 min. Then, solutions of the red Ir dendrimers without or with m-MTDATA in *o*-dichlorobenzene were filtered through a filter (0.45 μm) and spin-coated on PEDOT:PSS as the emissive layer (EML) at a speed of 1500 rpm for 60 s. Successively, the substrate was annealed at 100 °C for 30 min inside a

nitrogen-filled glovebox and then transferred to a vacuum thermal evaporator. On top of the EML, a 60 nm thick film of TmPyPB was thermally deposited at a pressure of 4.0×10^{-4} Pa. Finally, 0.5 nm LiF and 100 nm Al were deposited as the cathode through a shadow mask with an array of 14 mm^2 openings. The EL spectra and CIE coordinates were measured using a PR650 spectra colorimeter. The current–voltage and brightness–voltage curves of devices were measured using a Keithley 2400/2000 source meter and a calibrated silicon photodiode. The EQE was calculated from the luminance, current density and EL spectra assuming a Lambertian distribution. All the measurements were carried out at room temperature under ambient conditions.

Synthesis:

All solvents for chemical synthesis were refined according to the standard procedures. Carbazole-based dendrons including D1, D2, and D3 were synthesized according to the literature.¹⁴

Th-PQ-Br: A mixture of 3-acetylthiophene (2.0 g, 15.8 mmol), 2-amino-4'-bromobenzophenone (4.4 g, 15.8 mmol), diphenylphosphate (4.0 g, 15.8 mmol), and m-cresol (20 mL) was flushed with N_2 while stirring at room temperature for 30 min and then refluxed for 12 h at $140 \text{ }^\circ\text{C}$. The reaction mixture was distilled to remove m-cresol, diluted with dichloromethane and washed with 10% sodium hydroxide solution. The resultant organic layer was dried over anhydrous NaSO_4 and evaporated to remove the solvent. The residue was then purified by column chromatography on silica gel with hexane/ethylacetate (9:1) as eluent to furnish a

white powder Th-PQ-Br (4.0 g, 70.0%). ^1H NMR (400 MHz, CDCl_3) δ 8.16 (d, $J = 8.0$ Hz, 1H), 7.75 (dd, $J = 14.0, 7.8$ Hz, 3H), 7.71 – 7.63 (m, 4H), 7.47 (dd, $J = 8.7, 4.3$ Hz, 1H), 7.42 (d, $J = 8.3$ Hz, 3H), 7.16 (t, $J = 4.2$ Hz, 1H).

R-Br: $\text{IrCl}_3 \cdot 3\text{H}_2\text{O}$ (0.7 g, 2.0 mmol) and Th-PQ-Br (1.8 g, 5.0 mmol) were added to a 40 mL mixture of 2-ethoxyethanol (30 mL) and water (10 mL). The mixture was refluxed for 24 h and then poured into water. The solid was collected by filtration and dried in a vacuum to give the crude chloro-bridged dimer. Without further purification, the dimer was added to a mixture of silver trifluoroacetate (0.6 g, 2.2 mmol), Th-PQ-Br (0.7 g, 2.0 mmol), K_2CO_3 (0.4 g, 3.0 mmol) and mesitylene (20 mL). After reflux for 24 h, the mixture was poured into water, and extracted with dichloromethane. The organic layer was carefully washed with water and dried with Na_2SO_4 . The crude product was purified by chromatography on silica gel with hexane/dichloromethane (3:1) as eluent to furnish a red powder R-Br (1.8 g, 68.2%). ^1H NMR (400 MHz, C_6D_6) δ 8.44 (d, $J = 8.8$ Hz, 3H), 7.88 (s, 3H), 7.74 (d, $J = 8.3$ Hz, 3H), 7.70 (d, $J = 7.8$ Hz, 6H), 7.40 (s, 3H), 7.30 (d, $J = 5.7$ Hz, 6H), 7.26 – 7.18 (m, 3H), 6.96 (t, $J = 7.7$ Hz, 3H), 6.57 (d, $J = 4.5$ Hz, 3H).

D1-Br: A mixture of D1 (12.0 g, 42.9 mmol), 1,4-dibromobenzene (10.1 g, 42.9 mmol), CuI (0.4 g, 2.1 mmol) and K_2CO_3 (13.7 g, 64.4 mmol) in DMI (30 mL) was heated at 160 °C for 24 h under argon. After cooling to room temperature, the mixture was poured into water, and extracted with dichloromethane. The organic layer was

carefully washed with water and dried with Na₂SO₄. The crude product was purified by chromatography on silica gel with hexane/dichloromethane (4:1) as eluent to furnish a white powder D1-Br (13.0 g, 70.0%). ¹H NMR (400 MHz, CDCl₃): δ 8.13 (d, *J* = 1.5 Hz, 2H), 7.70 (d, *J* = 8.6 Hz, 2H), 7.46 (dd, *J* = 8.3, 1.9 Hz, 2H), 7.43 (d, *J* = 6.1 Hz, 2H), 7.31 (d, *J* = 8.6 Hz, 2H), 1.46 (s, 18H).

D2-Br: This compound was prepared according to the procedure for the synthesis of D1-Br by using D2 instead of D1 in a yield of 72.0%. ¹H NMR (400 MHz, CDCl₃) δ 8.23 (d, *J* = 1.8 Hz, 2H), 8.15 (d, *J* = 1.7 Hz, 4H), 8.02 (d, *J* = 8.3 Hz, 2H), 7.65 (d, *J* = 8.7 Hz, 2H), 7.59 (dd, *J* = 8.7, 2.0 Hz, 2H), 7.43 (dd, *J* = 8.7, 1.9 Hz, 4H), 7.34 (d, *J* = 8.6 Hz, 4H), 1.46 (s, 36H).

D3-Br: This compound was prepared according to the procedure for the synthesis of D1-Br by using D3 instead of D1 in a yield of 63.2%. ¹H NMR (400 MHz, CDCl₃) δ 8.56 (s, 2H), 8.31 (d, *J* = 8.5 Hz, 2H), 8.27 (d, *J* = 1.5 Hz, 4H), 8.15 (d, *J* = 1.7 Hz, 8H), 7.92 (d, *J* = 8.4 Hz, 2H), 7.74 (s, 4H), 7.63 – 7.56 (m, 8H), 7.43 (dd, *J* = 8.7, 1.9 Hz, 8H), 7.34 (d, *J* = 8.6 Hz, 8H), 1.46 (s, 72H).

D1-B: D1-Br (5.4 g, 12.4 mmol), bis(pinacolato)diboron (7.8 g, 31.1 mmol), Pd(dppf)Cl₂ (0.2 g, 0.3 mmol), and KOAc (3.7 g, 37.3 mmol) were added to a clean dry three-neck flask filled with argon. 30 mL N,N-dimethylformamide was added into the mixture. Then the solution was stirred at 100 °C for 12 h. After cooling to room

temperature, 100 mL water was slowly added to the solution. The mixture was filtered and the residue was washed with water and dried in a vacuum and then purified by column chromatography on silica gel with hexane/ethyl acetate (20:1) as eluent to furnish a white powder D1-B (5.7 g, 96.0%). $^1\text{H NMR}$ (400 MHz, CDCl_3) δ 8.13 (d, $J = 1.5$, 2H), 8.02 (d, $J = 8.2$, 2H), 7.58 (d, $J = 8.2$, 2H), 7.46 (dd, $J = 8.7$, 1.8, 2H), 7.39 (d, $J = 8.7$, 2H), 1.46 (s, 18H), 1.40 (s, 12H).

D2-B: This compound was prepared according to the procedure for the synthesis of D1-B by using D2-Br instead of D1-Br in a yield of 87.5%. $^1\text{H NMR}$ (400 MHz, CDCl_3) δ 8.23 (d, $J = 1.8$ Hz, 2H), 8.15 (d, $J = 1.7$ Hz, 4H), 7.75 (d, $J = 8.3$ Hz, 2H), 7.66 (d, $J = 8.7$ Hz, 2H), 7.59 (dd, $J = 8.7$, 2.0 Hz, 2H), 7.45 (dd, $J = 8.7$, 1.9 Hz, 4H), 7.33 (d, $J = 8.6$ Hz, 4H), 1.46 (s, 36H), 1.42 (s, 12H).

D3-B: This compound was prepared according to the procedure for the synthesis of D1-B by using D3-Br instead of D1-Br in a yield of 82.9%. $^1\text{H NMR}$ (400 MHz, CDCl_3) δ 8.56 (s, 2H), 8.31 (d, $J = 8.5$ Hz, 2H), 8.27 (d, $J = 1.5$ Hz, 4H), 8.15 (d, $J = 1.7$ Hz, 8H), 8.04 (d, $J = 8.4$ Hz, 2H), 7.87 (s, 4H), 7.68 – 7.57 (m, 8H), 7.45 (dd, $J = 8.7$, 1.9 Hz, 8H), 7.34 (d, $J = 8.6$ Hz, 8H), 1.45 (s, 72H), 1.42 (s, 12H).

R-D1: Compound R-Br (0.3 g, 0.2 mmol), D1-Br (0.5 g, 1.1 mmol), $\text{Pd}_2(\text{dba})_3$ (16 mg, 0.018 mmol) and s-Phos (59 mg, 0.14 mmol) were dissolved in 30 mL mesitylene, an aqueous solution of 2M K_2CO_3 (1 mL, 2 mmol) and one drop of Aliquat 336 was

added to the solution and then the mixture was heated to 100 °C for 12 h under argon. After cooled to room temperature, 50 mL dichloromethane was added to the solution. The organic phase was washed with water and dried with anhydrous Na₂SO₄. Solvents were removed under vacuum and the residue was purified by column chromatography over silica gel with hexane/dichloromethane (2:1) as the eluent to give the product as a red solid (0.3g, 74.2%). ¹H NMR (400 MHz, CDCl₃) δ 8.17 (d, *J* = 1.4 Hz, 9H), 7.89 (t, *J* = 8.4 Hz, 15H), 7.74 (d, *J* = 3.5 Hz, 6H), 7.73 – 7.66 (m, 9H), 7.50 (dd, *J* = 8.7, 1.8 Hz, 6H), 7.45 (d, *J* = 8.6 Hz, 6H), 7.21 (d, *J* = 4.7 Hz, 6H), 6.90 – 6.81 (m, 3H), 6.16 (d, *J* = 4.8 Hz, 3H), 1.49 (s, 54H). ¹³C NMR (400 MHz, CDCl₃) δ 161.86, 158.87, 149.45, 149.23, 143.04, 140.62, 139.21, 138.90, 138.22, 137.85, 137.03, 134.76, 130.41, 129.74, 128.71, 128.45, 127.52, 127.25, 127.05, 126.29, 125.02, 124.73, 123.70, 123.53, 118.26, 116.32, 109.31, 34.79, 32.06. MS (MALDI-TOF) *m/z*: 2110.81 [M⁺]. Anal. Calcd. for C₁₃₅H₁₁₇IrN₆S₃: C, 76.78; H, 5.58; N, 3.98. Found: C, 76.18; H, 5.94; N, 3.37.

R-D2: This compound was prepared according to the procedure for the synthesis of R-D1 by using D2-B instead of D1-B in a yield of 65.1%. ¹H NMR (400 MHz, CDCl₃) δ 8.27 (t, *J* = 4.0 Hz, 6H), 8.18 (t, *J* = 5.5 Hz, 15H), 8.01 (d, *J* = 8.5 Hz, 6H), 7.90 (dt, *J* = 18.1, 9.1 Hz, 15H), 7.81 – 7.70 (m, 15H), 7.64 (dd, *J* = 8.7, 1.9 Hz, 6H), 7.52 – 7.42 (m, 12H), 7.39 – 7.31 (m, 12H), 7.24 – 7.17 (m, 6H), 6.93 – 6.81 (m, 3H), 6.16 (dd, *J* = 10.3, 3.1 Hz, 3H), 1.47 (m, 108H). ¹³C NMR (400 MHz, CDCl₃) δ 161.85, 158.89, 149.44, 149.13, 142.59, 140.35, 140.14, 138.19, 137.31, 136.81, 134.74,

131.02, 130.48, 129.75, 128.86, 128.76, 127.55, 127.35, 126.25, 126.03, 124.86, 124.57, 124.10, 123.58, 123.15, 119.35, 118.27, 116.23, 111.21, 109.09, 34.73, 32.05. MS (MALDI-TOF) m/z : 3437.54 [M^+]. Anal.Calcd. for $C_{231}H_{207}IrN_{12}S_3$: C, 80.66; H, 6.07; N, 4.89. Found: C, 81.12; H, 5.94; N, 4.37.

R-D3: This compound was prepared according to the procedure for the synthesis of R-D1 by using D3-B instead of D1-B in a yield of 54.1%. 1H NMR (400 MHz, $CDCl_3$) δ 8.58 (s, 6H), 8.28 (s, 12H), 8.23 – 8.13 (m, 30H), 8.10 (d, $J = 8.1$ Hz, 6H), 7.96 (t, $J = 7.8$ Hz, 12H), 7.89 (q, $J = 8.8$ Hz, 15H), 7.85 – 7.75 (m, 12H), 7.64 (dd, $J = 18.9, 8.6$ Hz, 24H), 7.45 (d, $J = 8.6$ Hz, 24H), 7.35 (d, $J = 8.6$ Hz, 14H), 7.23(s,10H), 6.98 – 6.80 (m, 3H), 6.18 (d, $J = 4.6$ Hz, 3H), 1.46 (s, 216H). ^{13}C NMR (400 MHz, $CDCl_3$) δ 161.92, 158.97, 149.50, 149.13, 142.59, 141.41, 141.17, 140.68, 140.25, 138.24, 137.54, 136.54, 130.83, 130.62, 130.20, 129.11, 127.77, 127.46, 126.53, 126.08, 124.91, 124.31, 123.85, 123.60, 123.16, 120.08, 119.47, 116.26, 111.88, 111.72, 109.15, 34.77, 32.09. MS (MALDI-TOF) m/z : 6091.98 [M^+]. Anal.Calcd. for $C_{423}H_{387}IrN_{24}S_3$: C, 83.35; H, 6.40; N, 5.52. Found: C, 83.21; H, 6.49; N, 5.37.

Author Information:

*Corresponding authors: junqiaod@ciac.ac.cn; lixiang@ciac.ac.cn

Acknowledgements

The authors acknowledge the financial support from the National Key Research and

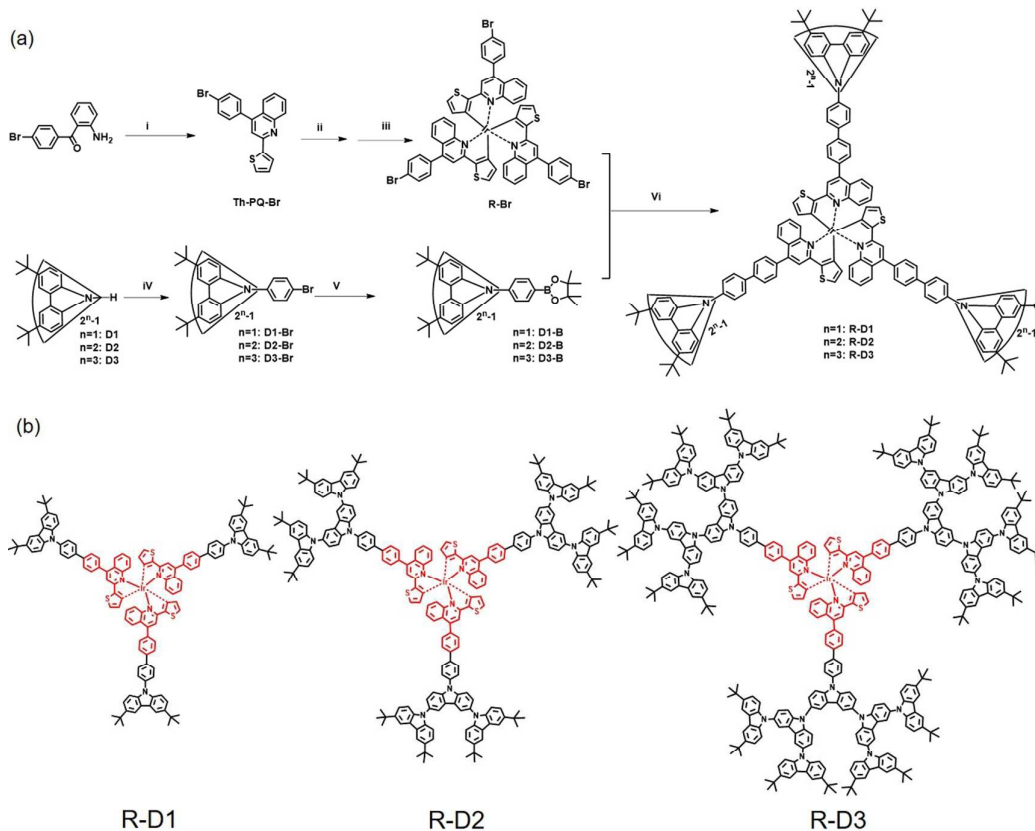
Development Program (2016YFB0401301), the 973 Project (2015CB655001) and the Natural Science Foundation of China (Nos. 51573183, 21604083 and 91333205).

References:

1. A. Sandstrom, H. F. Dam, F. C. Krebs and L. Edman, *Nat. Commun.*, 2012, **3**, 1002.
2. H. Zheng, Y. Zheng, N. Liu, N. Ai, Q. Wang, S. Wu, J. Zhou, D. Hu, S. Yu, S. Han, W. Xu, C. Luo, Y. Meng, Z. Jiang, Y. Chen, D. Li, F. Huang, J. Wang, J. Peng and Y. Cao, *Nat. Commun.*, 2013, **4**, 1971.
3. J. Birnstock, J. Blässing, A. Hunze, M. Scheffel, M. Stöbel, K. Heuser, G. Wittmann, J. Wörle and A. Winnacker, *Appl. Phys. Lett.*, 2001, **78**, 3905.
4. F. Villani, P. Vacca, G. Nenna, O. Valentino, G. Burrasca, T. Fasolino, C. Minarini and D. Sala, *J. Phys. Chem. C* 2009, **113**, 13398.
5. T. Giridhar, T. H. Han, W. Cho, C. Saravanan, T. W. Lee and S. H. Jin, *Chem. Eur. J.*, 2014, **20**, 8260.
6. N. Aizawa, Y. J. Pu, M. Watanabe, T. Chiba, K. Ideta, N. Toyota, M. Igarashi, Y. Suzuri, H. Sasabe and J. Kido, *Nat. Commun.*, 2014, **5**, 5756.
7. S. H. Hwang, C. N. Moorefield and G. R. Newkome, *Chem. Soc. Rev.*, 2008, **37**, 2543.
8. S. C. Lo and P. L. Burn, *Chem. Rev.*, 2007, **107**, 1097.
9. A. W. Freeman, S. C. Koene, P. R. L. Malenfant, M. E. Thompson and J. M. J. Fréchet, *J. Am. Chem. Soc.*, 2000, **122**, 12385.

10. X. -Y. Deng, *Int. J. Mol. Sci.*, 2011, **12**, 1575.
11. S. -Y. Shao, J. -Q. Ding and L. -X. Wang, *Chin. Chem. Lett.*, 2016, **27**, 1201.
12. M. -M. Sun, W. Wang, L. -Y. Liang, S. -H. Yan, M. -L. Zhou and Q. -D. Ling, *Chin. J. Polym. Sci.*, 2015, **33**, 783.
13. Q. D. Ling, M. J. Yang, W. Wang, M. J. Lin and W. G. Zhang, *Acta. Chim. Sinica*, 2005, **63**, 637.
14. J. Q. Ding, J. H. Lu, Y. X. Cheng, Z. Y. Xie, L. X. Wang, X. B. Jing and F. S. Wang, *Adv. Funct. Mater.*, 2008, **18**, 2754.
15. L. C. Chen, S. M. Wang, Z. M. Yan, J. Q. Ding, L. X. Wang, *J. Mater. Chem. C*, 2017, **5**, 5749.
16. J. Q. Ding, B. Wang, Z. Y. Yue, B. Yao, Z. Y. Xie, Y. X. Cheng, L. X. Wang, X. B. Jing and F. S. Wang, *Angew. Chem. Int. Ed.*, 2009, **48**, 6664.
17. J. Q. Ding, J. Gao, Y. X. Cheng, Z. Y. Xie, L. X. Wang, D. G. Ma, X. B. Jing and F. S. Wang, *Adv. Funct. Mater.*, 2006, **16**, 575.
18. D. B. Xia, B. Wang, B. Chen, S. M. Wang, B. H. Zhang, J. Q. Ding, L. X. Wang, X. B. Jing and F. S. Wang, *Angew. Chem. Int. Ed.*, 2014, **53**, 1048.
19. Y. Wang, S. M. Wang, S. Y. Shao, J. Q. Ding, L. X. Wang, X. B. Jing and F. S. Wang, *Dalton Trans.*, 2015, **44**, 1052.
20. M. Zhang, S. Xue, W. Dong, Q. Wang, T. Fei, C. Gu and Y. Ma, *Chem. Commun.*, 2010, **46**, 3923.
21. J. Q. Ding, J. Gao, Q. Fu, Y. X. Cheng, D. G. Ma and L. X. Wang, *Synth. Met.*, 2005, **155**, 539.

22. H. Y. Oh, C. Kulshreshtha, J. H. Kwon and S. Lee, *Org. Electron.*, 2010, **11**, 1624.
23. M. R. Zhu, T. L. Ye, X. He, X. S. Cao, C. Zhong, D. G. Ma, J. G. Qin and C. L. Yang, *J. Mater. Chem.*, 2011, **21**, 9326.
24. M. R. Zhu, Y. H. Li, S. J. Hu, C. G. Li, C. L. Yang, H. B. Wu, J. G. Qin and Y. Cao, *Chem. Commun.*, 2012, **48**, 2695.
25. S. M. Wang, X. D. Wang, B. Yao, B. H. Zhang, J. Q. Ding, Z. Y. Xie and L. X. Wang, *Sci. Rep.*, 2015, **5**, 12478.
26. D. D. Zhang, L. Duan, D. Q. Zhang, Y. Qiu, *J. Mater. Chem. C*, 2014, **2**, 8983.

Scheme 1. Synthetic route (a) and molecular structures (b) of the red Ir dendrimers.

Reagents and conditions: (i) 3-acetylthiophene, DPP, *m*-cresol; (ii) iridium(III) chloride trihydrate, water, 2-ethoxyethanol, reflux; (iii) silver trifluoroacetate, Th-PQ-Br, K_2CO_3 , mesitylene, reflux; (iv) 1,4-dibromobenzene, CuI, K_2CO_3 , DMI, 160 °C; (v) bis(pinacolato)diboron, $Pd(dppf)Cl_2$, KOAc, DMF, 80 °C; (vi) $Pd_2(dba)_3$, S-Phos, 2M K_2CO_3 , mesitylene, 100 °C.

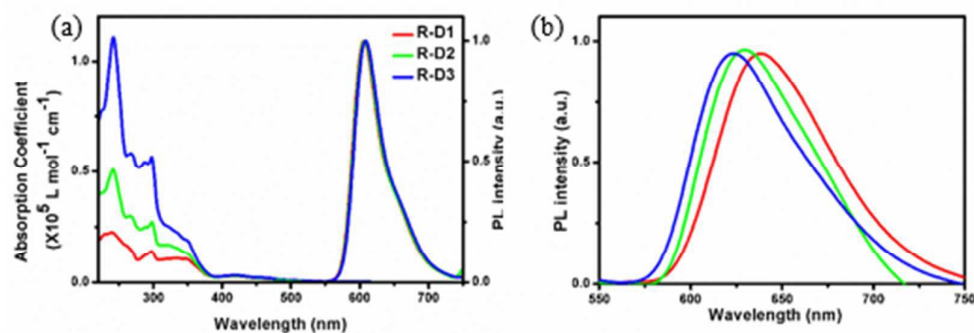


Figure 1. Photophysical properties of the red Ir dendrimers R-D1 ~ R-D3: (a) UV-Vis absorption spectra in dichloromethane and PL spectra in toluene at a concentration of 10^{-5} M; (b) PL spectra in solid films.

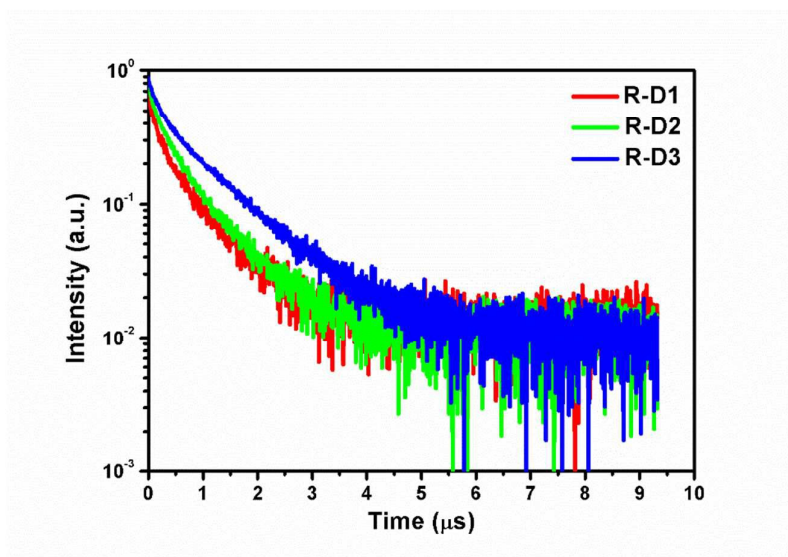


Figure 2. Transient PL spectra of the red Ir dendrimers R-D1 ~ R-D3 in solid films.

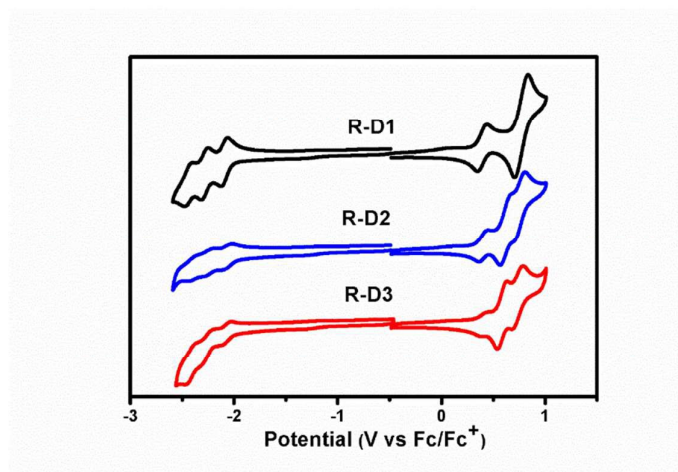


Figure 3. CV curves of the red Ir dendrimers R-D1 ~ R-D3.

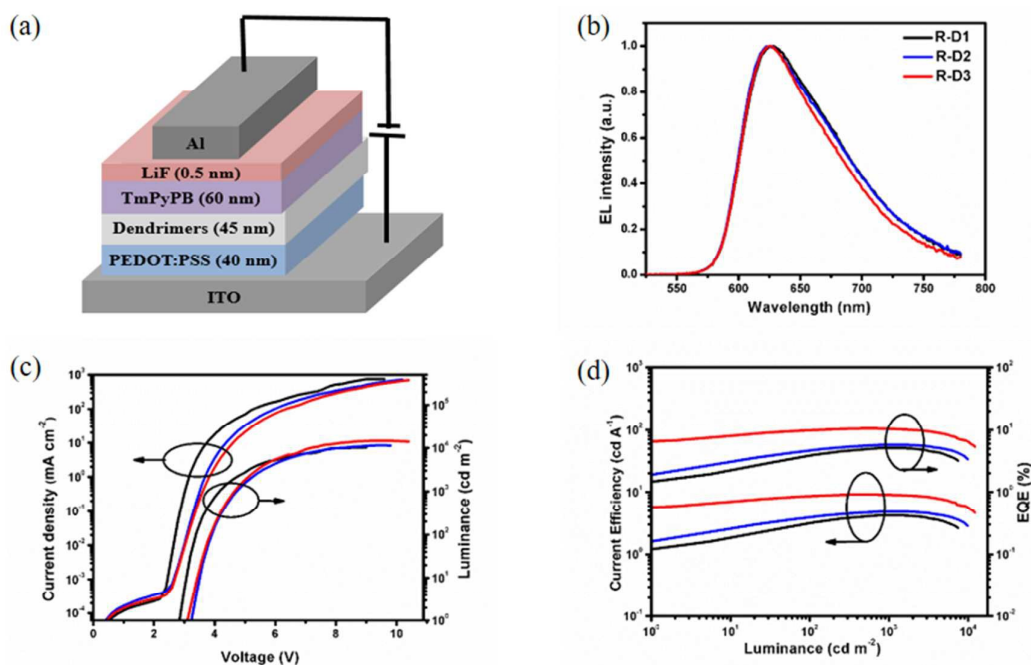


Figure 4. Nondoped device performance for the red Ir dendrimers R-D1 ~ R-D3 : (a) device configuration; (b) EL spectra at 6 V; (c) current density–voltage–luminance characteristics; (d) luminance dependence on the current efficiency and EQE.

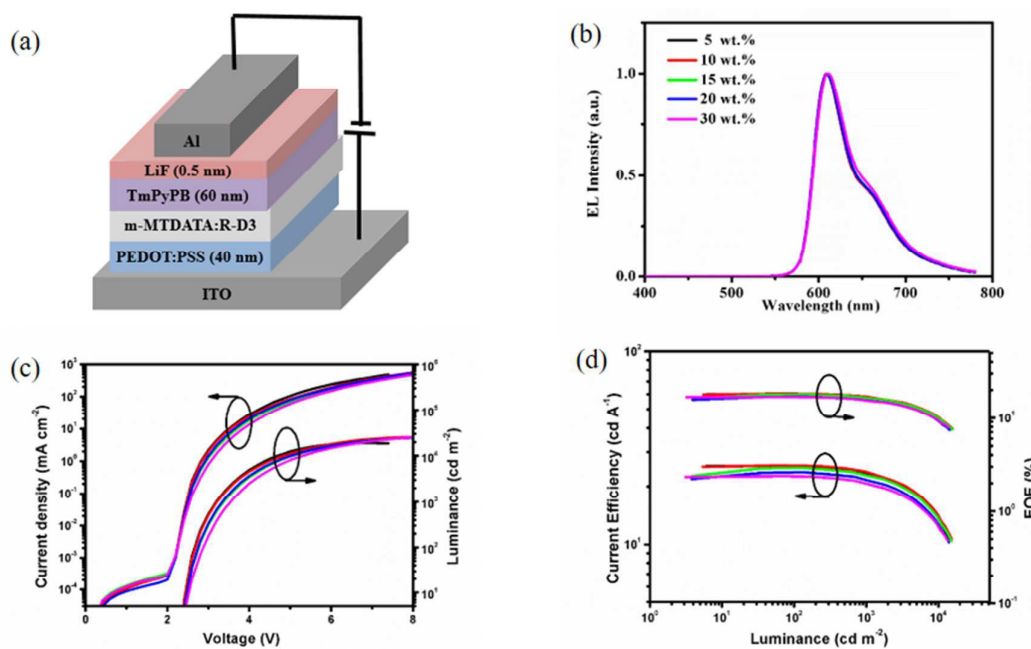


Figure 5. Doped device performance for the third-generation dendrimer R-D3: (a) device structure; (b) EL spectra at 6 V; (c) current density–voltage–luminance characteristics; (d) luminance dependence on the current efficiency and EQE.

Table 1. Photophysical, electrochemical and thermal properties of the red Ir dendrimers.

Dendrimer	$\lambda_{\text{abs}} (\log \epsilon)^{\text{a}}$ (nm)	$\lambda_{\text{em}}^{\text{b}}$ (nm)	$\lambda_{\text{em}}^{\text{c}}$ (nm)	$\Phi_{\text{PL}}^{\text{d}}$	τ^{e} (μs)	HOMO ^f (eV)	LUMO ^f (eV)	T _d (°C)	T _g (°C)
R-D1	240 (5.3), 297 (5.1), 349 (5.0), 418 (4.5), 462 (4.4), 586 (3.4)	606	639	0.42	0.54	-5.12	-2.79	470	199
R-D2	242 (5.7), 267 (5.5), 298 (5.4), 349 (5.1), 420 (4.5), 461 (4.3), 585 (3.4)	607	630	0.42	0.59	-5.13	-2.80	526	n.d.
R-D3	242 (6.0), 269 (5.8), 297 (5.8), 348 (5.3), 419 (4.5), 463 (4.3), 585 (3.3)	609	624	0.40	0.92	-5.13	-2.81	530	n.d.

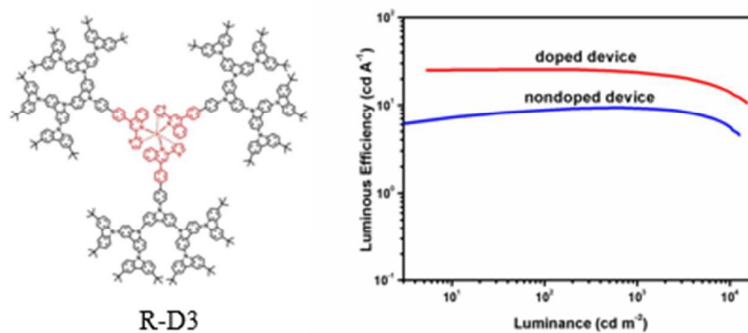
^a Measured in dichloromethane at a concentration of 10^{-6} M; ^b Measured in toluene at a concentration of 10^{-5} M; ^c Measured in solid films; ^d Measured in degassed toluene with *fac*-Ir(ppy)₃ ($\Phi_{\text{PL}} = 0.97$) as the reference; ^e Measured in solid films degassed by N₂; ^f HOMO = $-e(E_{\text{ox}} + 4.8 \text{ V})$, LUMO = $-e(E_{\text{red}} + 4.8 \text{ V})$, where E_{ox} and E_{red} are the onset values from the first oxidation and reduction waves, respectively.

Table 2. Device performance for the red Ir dendrimers.

Device	V_{on}^a (V)	L_{max}^b ($cd\ m^{-2}$)	LE ^c ($cd\ A^{-1}$)	PE ^d ($lm\ W^{-1}$)	EQE ^e (%)	CIE (x, y)
R-D1	3.0	10290	4.2/3.2/4.2	3.3/3.0/3.2	5.1/3.9/5.1	(0.67,0.33)
R-D2	3.2	11470	4.8/3.6/4.8	3.3/3.0/3.3	5.7/4.3/5.6	(0.67,0.33)
R-D3	3.2	14810	9.2/8.5/9.1	7.0/7.0/6.9	10.5/9.7/10.1	(0.67,0.33)
R-D3 (5 wt.%)	2.4	18990	25.6/25.5/23.2	33.2/29.6/22.7	18.1/18.1/16.4	(0.65,0.34)
R-D3 (10 wt.%)	2.4	25270	25.7/25.6/23.9	33.0/29.9/23.4	18.3/18.2/17.0	(0.65,0.34)
R-D3 (15 wt.%)	2.4	25730	25.0/25.0/22.7	30.0/28.0/20.9	17.9/17.9/16.3	(0.65,0.34)
R-D3 (20 wt.%)	2.4	25080	23.7/23.7/21.3	28.6/26.6/19.7	17.0/17.0/15.3	(0.65,0.34)
R-D3 (30 wt.%)	2.4	26690	22.7/22.6/20.4	29.4/24.5/17.8	16.9/16.8/15.2	(0.66,0.34)

^a Turn-on voltage at a brightness of $1\ cd\ m^{-2}$; ^b The maximum brightness; ^c The current efficiency at maximum, 100 and $1000\ cd\ m^{-2}$; ^d The power efficiency at maximum, 100 and $1000\ cd\ m^{-2}$; ^e The external quantum efficiency at maximum, 100 and $1000\ cd\ m^{-2}$.

Table of Content



R-D3

Solution processible red Ir dendrimers have been demonstrated to give state-of-art current efficiencies as high as 9.2 and 25.7 cd/A for nondoped and doped PhOLEDs, respectively, which can compete well with vacuum-deposited small molecular phosphors.